

Tissue characterization using a phantom to validate four-dimensional tissue deformation

Martin Szegedi,^{a)} Prema Rassiah-Szegedi, and Vikren Sarkar
Huntsman Cancer Hospital, The University of Utah, Salt Lake City, Utah 84102

Jacob Hinkle
Scientific Computing and Imaging Institute, University of Utah, Salt Lake City, Utah 84112

Brian Wang, Yu-Huei Huang, and Hui Zhao
Huntsman Cancer Hospital, The University of Utah, Salt Lake City, Utah 84102

Sarang Joshi
Scientific Computing and Imaging Institute, University of Utah, Salt Lake City, Utah 84112

B. J. Salter
Huntsman Cancer Hospital, The University of Utah, Salt Lake City, Utah 84102

(Received 25 May 2012; revised 6 August 2012; accepted for publication 8 August 2012; published 18 September 2012)

Purpose: This project proposes using a real tissue phantom for 4D tissue deformation reconstruction (4DTDR) and 4D deformable image registration (DIR) validation, which allows for the complete verification of the motion path rather than limited end-point to end-point of motion.

Methods: Three electro-magnetic-tracking (EMT) fiducials were implanted into fresh porcine liver that was subsequently animated in a clinically realistic phantom. The animation was previously shown to be similar to organ motion, including hysteresis, when driven using a real patient's breathing pattern. For this experiment, 4DCTs and EMT traces were acquired when the phantom was animated using both sinusoidal and recorded patient-breathing traces. Fiducial were masked prior to 4DTDR for reconstruction. The original 4DCT data (with fiducials) were sampled into 20 CT phase sets and fiducials' coordinates were recorded, resulting in time-resolved fiducial motion paths. Measured values of fiducial location were compared to EMT measured traces and the result calculated by 4DTDR.

Results: For the sinusoidal breathing trace, 95% of EMT measured locations were within 1.2 mm of the measured 4DCT motion path, allowing for repeatable accurate motion characterization. The 4DTDR traces matched 95% of the EMT trace within 1.6 mm. Using the more irregular (in amplitude and frequency) patient trace, 95% of the EMT trace points fitted both 4DCT and 4DTDR motion path within 4.5 mm. The average match of the 4DTDR estimation of the tissue hysteresis over all CT phases was 0.9 mm using a sinusoidal signal for animation and 1.0 mm using the patient trace.

Conclusions: The real tissue phantom is a tool which can be used to accurately characterize tissue deformation, helping to validate or evaluate a DIR or 4DTDR algorithm over a complete motion path. The phantom is capable of validating, evaluating, and quantifying tissue hysteresis, thereby allowing for full motion path validation. © 2012 American Association of Physicists in Medicine. [<http://dx.doi.org/10.1118/1.4747528>]

Key words: validation, real tissue phantom, SBRT, 4D dose

I. INTRODUCTION

A widely used tool for characterizing patient-specific organ/tumor motion is four-dimensional computed tomography (4DCT). In addition to the accurate knowledge of patient-specific organ motion gained by use of 4DCT imaging, another application of recent interest is the calculation of a so-called "4D dose distribution" via the use of 4D tissue deformation reconstruction (4DTDR) and 4D deformable image registration (DIR).

Hinkle *et al.*¹ developed a 4DTDR algorithm by fitting a spatiotemporal motion model (STMM) to either raw CT projection data if available or unbinned CT-images. In order to alleviate artifacts resulting from binning errors, the 4DTDR performs a joint registration, wherein a STMM and a single

image are matched simultaneously to all the other images. Regularization of the motion model may then be used to diminish the impact of image artifacts on the resulting motion estimate. This approach allows reconstruction of a motion path at any time or position while providing a lower signal to noise ratio. Current studies²⁻⁶ are limited in their ability to verify measured spatial landmark continuously in time and therefore published data often use deformation endpoints. Deviations between DIR calculation and intermittent CT phase measurements on the motion path, i.e., before the motion path is completed, are usually neglected. Validation studies⁶ often evaluate the performance of DIR algorithms by comparing the position of high-contrast feature points against "ground truth" positions, thereby determining algorithms which easily identify points reliably. Since DIR and 4DTDR algorithms

each use image contrast to guide motion estimation, it is considerably more challenging to evaluate performance in low-contrast environments such as the interior of the liver. This work introduces a phantom with a low-contrast environment to measure the performance of a 4DTDR algorithm. Even though it is infeasible to track as many low-contrast points using fiducials as are commonly used in extracted-feature studies, the additional challenge provided by the lack of contrast makes such phantom use for validation quite useful.

The most meaningful validation for a given DIR or 4DTDR will require use of a deformable phantom capable of repeatable, realistic simulation of all important tissue specific behaviors, including voxel deformation and hysteresis. The phantom, a clinically realistic porcine liver phantom which is capable of producing patient equivalent tissue deformation,⁷ allows end-to-end validation of motion and a full analysis of the motion characteristic of the tissue in time and location of voxels. This real-tissue 4D phantom produces periodic 3D-motion, equivalent to that typically observed in patients, to validate the free-form diffeomorphism/smooth-velocity-flow 4DTDR model.¹

II. METHODS

A previously described motion phantom containing a porcine liver lobe⁷ with fiducials embedded for evaluation of a previously reported 4DTDR (Ref. 1) was used.

II.A. Data acquisition

The phantom was prepared with a freshly explanted porcine liver containing three electro-magnetic tracking (EMT) transponders (~8 mm long and 2 mm in diameter). A phantom motion-controller that runs sinusoidal and irreg-

ular patient-recorded breathing pattern, via a piston, was applied onto the liver. For this study, a sinusoidal 6 s trace or one specific patient trace were used. A GE Lightspeed RT16 CT scanner (GE Healthcare, Waukesha, WI) with the Real-time Position Management (RPM) system (Varian RPM, Varian Medical Systems Inc., Palo Alto, CA)⁸⁻¹⁰ was used for the 4DCT acquisition. Images were acquired using 1.25 mm slices while maximizing the number of images that can be obtained for a 4DCT dataset which is a maximum of 3000 images. The image number of 4DCT in this study ranged between 2880 and 2944 images. Image data were processed using the GE AW Sim MD software (version 7.6) to generate 20 separate phase-binned CT image sets, depending on the length of couch movement during data acquisition. This 4DCT data were then used to generate a complete motion path for each fiducial.

In order to confirm the accurate 4DCT measurement of fiducial motion, and to understand the natural variation of motion within tissue, the phantoms' complete motion was tracked for multiple periods using an EMT localizing and tracking system (Calypso Medical Technologies Inc., Seattle, WA) based in our treatment vault. Figure 1 shows the setup of the phantom. In each case, the animation lasted approximately 10 min. The EMT generated data (10 Hz for individual transponders), utilizing a higher temporal positional acquisition rate than 4DCT, were compared to the 4DCT measured fiducial coordinates motion pattern and, ultimately, to the 4DTDR predicted motion pattern.

II.B. Data processing

Data points in the phase sampled CT data were analyzed manually by one person. Data points in the 4DTDR were

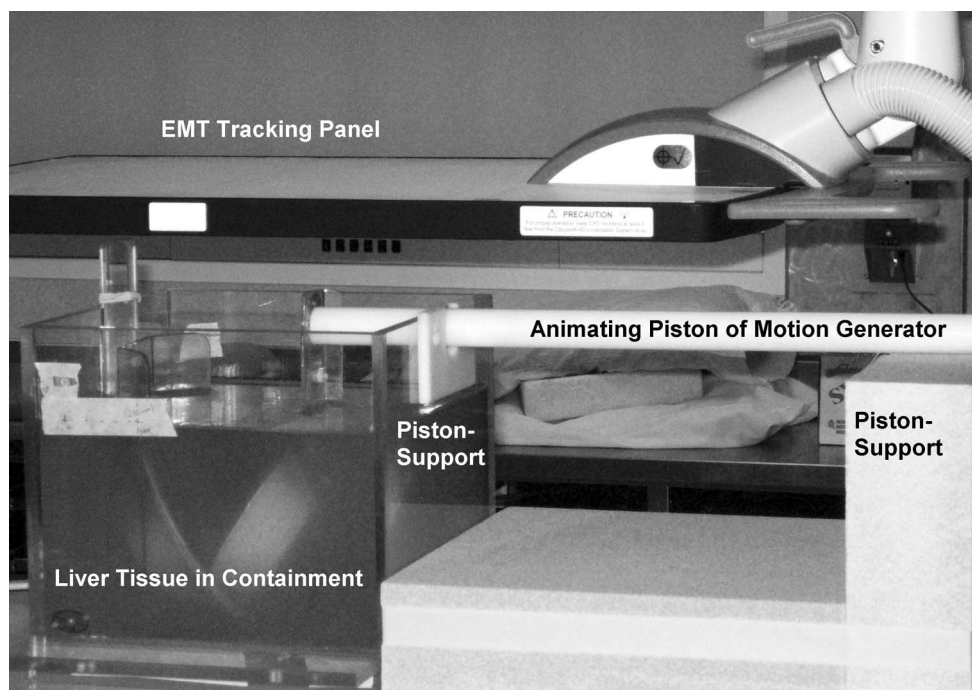


FIG. 1. Image of liver phantom setup in the treatment vault for EMT trace recording.

acquired through software means. To create a spatiotemporal link between 4DCT and 4DTDR generated data, the piston position was used as a common reference point to map the 4DCT phase-based data into the temporal/amplitude-based frame of the 4DTDR. The EMT fiducials' locations were compared against the motion pattern generated by the respective fiducial in the phase binned 4DCT data. The 4DTDR predicted fiducial motion patterns were calculated and compared against 4DCT motion pattern. To confirm the accuracy of the 4DCT measurement, which represents the “ground truth” for comparison with the 4DTDR, the shortest 3D-distance of each EMT trace point to the interpolated CT-phase binned motion track was calculated. Good agreement of the 4DCT with the high temporal resolution EMT indicates accurate (i.e., artifact free) 4DCT measurement of fiducial motion patterns.

II.C. Maximum *a posteriori* (MAP) 4D tissue deformation reconstruction

We used all raw, time-stamped 4D images to reconstruct and estimate deformations in anatomy, outlined in detail by Hinkle *et al.*¹ Using the breathing trace from the RPM system, along with the data time-stamps, the raw image data were tagged with a breathing-signal amplitude. For a periodic breathing pattern under conditions of hysteresis, a given voxel's trajectory essentially corresponds to tracing one half of an approximately elliptical 3D path whenever the breathing signal is rising (exhale), and the other half when the breathing signal is falling (inhale). Using two-parameter binning methods (Langner and Keall¹¹), we found that the time derivative of the breathing signal, in combination with the breathing signal itself, gave the best parameterization. Therefore, the 4DTDR_{hysteresis} received partitioned data, i.e., two disjoint sets—one with positive breathing signal and one with negative breathing signal derivative. The resulting two, amplitude-index motion estimates were then jointly estimated, along with a common base image.

II.D. Electronic masking of fiducials in porcine liver

To avoid the possibility of any algorithm, as well as the 4DTDR benefiting from the unfair advantage of being “driven” by the implanted fiducials, the fiducials were masked in a second dataset. Images containing fiducials or clearly visible artifacts of fiducials were processed prior to being submitted to the 4DTDR. A rectangular region encompassing the streak artifacts centered around each fiducial was outlined and a homogeneous region of equivalent size, containing unaliased liver tissue, was chosen in the same slice and tiled into the erased region. After tiling and successful visual verification of fiducial masking, pixels along the edges of the masked region were blended with their original values using a Tukey (cosine taper) window function. This resulted in the slices being effectively masked of evidence of the fiducials, while retaining the texture of homogenous liver tissue.

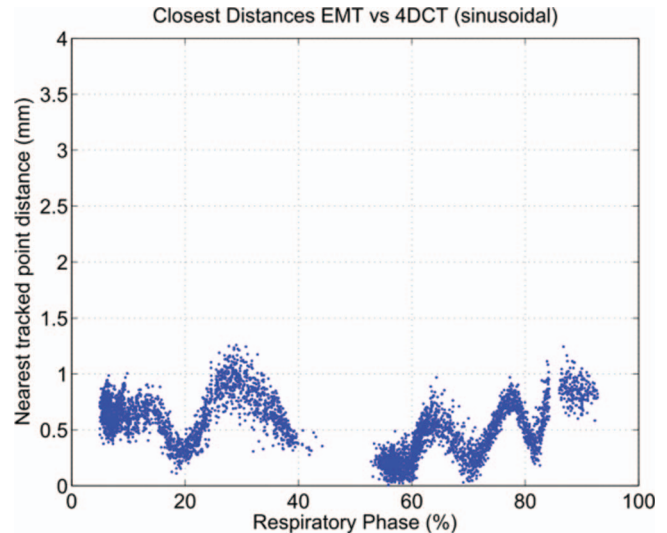


FIG. 2. Comparison of EMT measurement of fiducial positions vs 4DCT marker tracking for sinusoidal trace animation.

III. RESULTS

III.A. Comparison of 4DCT measurement to EMT tracking measurement

The accuracy of the EMT system has been reported to be less than 0.5 mm in any direction for motion speeds of up to 3 cm/s.¹² Ninety-five percent and ninety-nine percent of the EMT points were within 1.2 mm and 1.4 mm of the 4DCT measurements. Figures 2 and 3 plot the 3D distances of the acquired EMT points to the closest 4DCT points (Y axis) according to respiratory phase for both 4DCT datasets. The sinusoidal animated liver indicates good agreement between the two measurement techniques as depicted in Fig. 2. The good reproducibility of liver tissue motion results in the EMT trace clustering nicely, rarely displaying greater than 1 mm difference. The same tissue, animated with the recorded

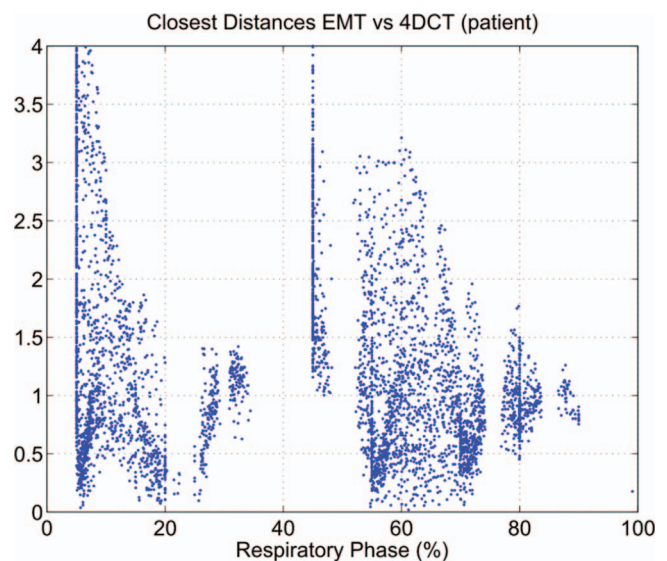


FIG. 3. Comparison of EMT measurement of fiducial positions vs 4DCT marker tracking for patient trace animation.

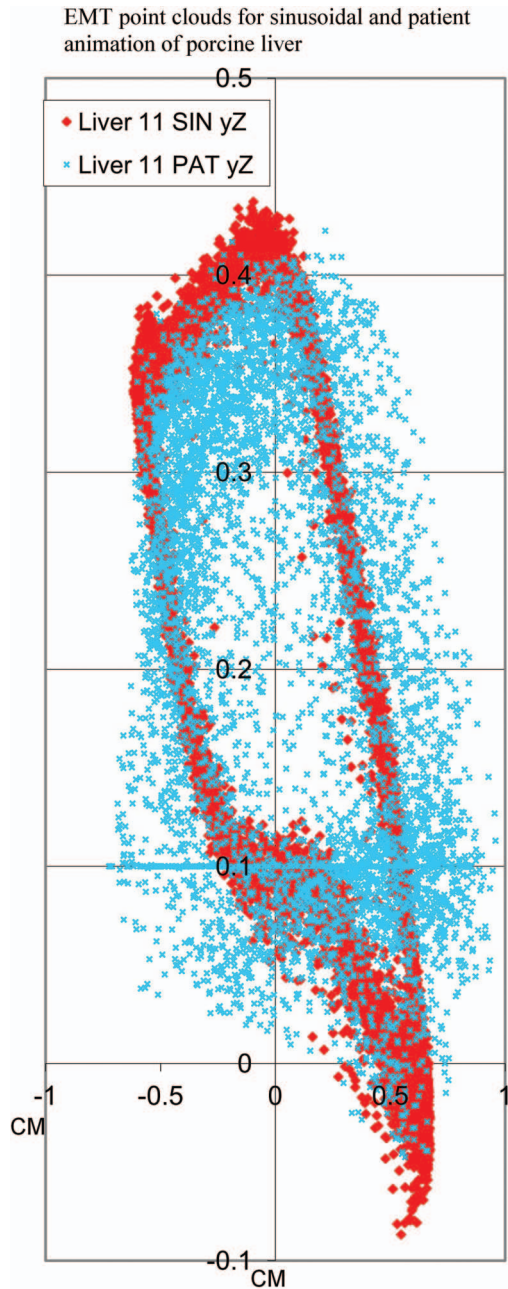


FIG. 4. EMT point clouds for sinusoidal (dark gray) and patient (light gray) animation of the same porcine liver in two dimensions.

patient trace can be seen in Fig. 3, showing a greater motion variation. The difference in sinusoidal and patient animation is visualized in Fig. 4 which depicts an example of the EMT point clouds for the clustered distinct sinusoidal (dark gray) and more varied patient (light gray) animation of the porcine liver in two dimensions. The wider spread of motion is in line with the variation in amplitude and period.

III.B. Measurement errors

Our error analysis revealed that the standard deviation of fiducial position measurements is submillimeter. We were able to localize the center of a stationary BB from all CT-

4DTDR calculated trajectory of a fiducial (solid) and the same data set calculated with masked fiducial (dashed)

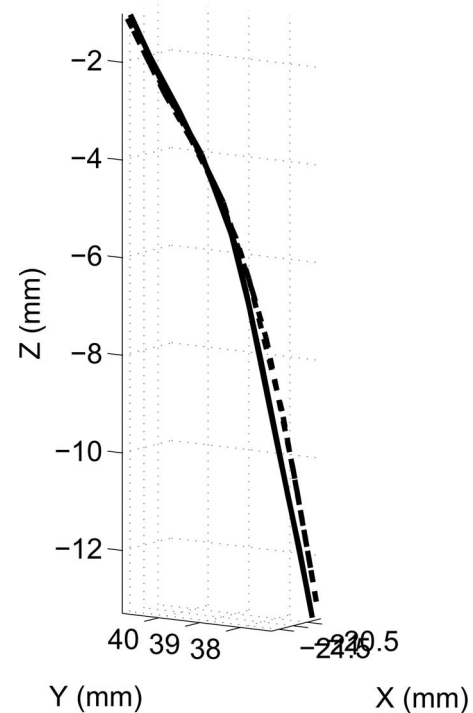


FIG. 5. 4DTDR tracks calculated from 4DCT (straight line) and 4DCT with masked fiducials (dotted lines).

phases with 0.1 mm standard deviation, at 1.25 mm slice thickness. The maximum phase sampling error (MPSE) for the sinusoidal 4DCT datasets after binning, as stated by the AW software, was 1% indicating correct phase assignment. Figure 5 displays the 4DTDR estimations of the 4DCT dataset with fiducials visible (lined track) and masked (dotted track). For same datasets the two corresponding 4DTDR motion paths were less than 0.1 mm, thus indicating that masking the fiducials is acceptable. For the purpose of this study, we therefore continued with the masked dataset results only.

III.C. Comparison of EMT tracking to the 4DTDR_{hysteresis} prediction, i.e., with breathing trace derivative

The 4DTDR_{hysteresis} solution, incorporating the RPM time derivative, resulted in a 0.9 mm average 3D distance from the measured sinusoidal animated 4DCT phase datasets with fiducials. The distances for the 95% and 99% of EMT points to the patient trace animated measured 4DCT data, 4DTDR and 4DTDR_{hysteresis} are shown in Table I. The 4DTDR_{hysteresis} results are close to the actual measurement. Figures 6 and 7 plot the 3D distances of the acquired EMT points to the closest 4DTDR_{hysteresis} points (Y axis) according to respiratory phase for both 4DTDR datasets. The 4DTDR_{hysteresis} calculated solution in Fig. 6 is comparing favorably with the distances measured between EMT and 4DCT data as shown in Fig. 2.

TABLE I. Percentile 3D distances of the EMT trace points in millimeter distance to 4DCT and 4DTDR points.

Percentile of EMT points	4DCT data	4DTDR	4DTDR _{hysteresis}
95%	1.2 mm	2.8 mm	1.0 mm
99%	1.4 mm	3.0 mm	1.2 mm

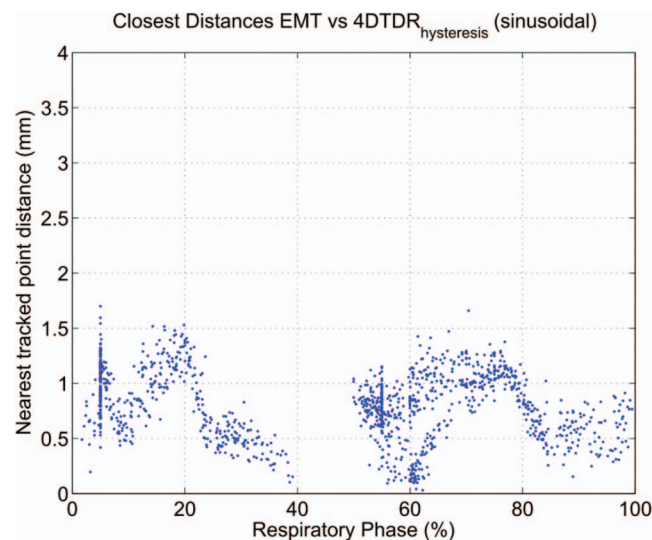
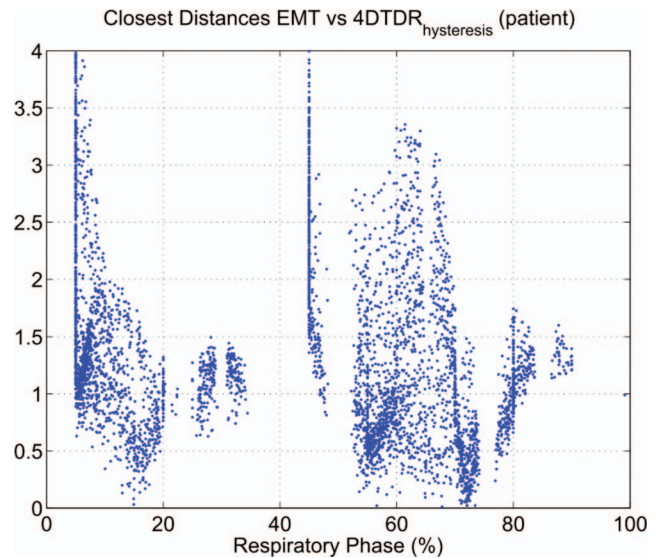
III.D. Comparison of EMT tracking to the 4DTDR_{hysteresis} prediction with patient trace-based animation

The MPSE for the patient-trace animated 4DCT dataset after binning, as stated by the AW software, was 13% indicating average phase assignment error, similar to real patient data on any day.

Numeric data, representing the 3D distance between measured 4DCT and 4DTDR_{hysteresis} (sinusoidal) and 4DTDR_{hysteresis} (patient) is presented in Table II. The 3D distances of the acquired EMT points to the closest 4DTDR_{hysteresis} points (Y axis) according to respiratory phase for the patient animated data in Fig. 7 again compare favorably to the EMT to 4DCT comparison in Fig. 3.

IV. DISCUSSION

Multiple studies have used limited sets of retrospective patient data (between 2 and 5) from 4DCT acquisition to validate their respective deformation models.^{13–15} These and other authors have gleaned their results from centroid-to-centroid comparison,¹⁶ volume-overlap-comparison, image cross-correlation, distance to agreement of manually/visually identified landmarks or organ-contours in 2D as well as in 3D, isointensity contours,^{17,18} and other similar measures. Average end to end errors in such studies are reported to range from 2 to 3 mm, but it is important to note that none of the

FIG. 6. Comparison of EMT measurement of fiducial positions vs 4DTDR_{hysteresis} estimation for sinusoidal trace animation.FIG. 7. Comparison of EMT measurement of fiducial positions vs 4DTDR_{hysteresis} estimation for patient trace animation.

mentioned methods report on the complete motion path accuracy, neither do they enable repeated motion characterization or can they account for errors in the widest part of the hysteresis loop.

To avoid the limitations of patient-based studies on the motion path and binning artifacts, a biologically realistic phantom-based validation is performed here using highly reproducible liver tissue motion. The capability of repeatedly modeling and characterizing real tissue hysteresis and deformation using a biologically realistic phantom as performed here improves validation efforts and counters challenges to the evaluation through imaging limitations on real patients.

Previously observed hysteresis in patients^{4,19} was challenging to reproduce and to accurately image repeatedly. Phantoms lacked a natural tissue hysteresis and were limited due to simplified tissue modeling approaches. A characterized hysteresis pattern in real tissue allows for study of behaviors when faced with irregular motion. The evaluated 4DTDR_{hysteresis} motion path fitted to measured regular 4DCT and EMT data to within less than 2 mm on average, i.e., the error here applies to any point within the motion path and not only to motion end points. More importantly, the phantom through the accurate characterization and repeatable measurements of tissue deformation allows validation of any deformative algorithm in detail.

TABLE II. 3D deviation of 4DTDR_{hysteresis} to 4DCT measured points.

Sum 3D vector Δ [mm]	4DTDR _{hysteresis} (sin.)	4DTDR _{hysteresis} (pat.)
Average error	0.9	1.0
Maximum error	2.0	1.6

V. CONCLUSION

Accurate validation over the whole motion path is essential in evaluating the usefulness of any DIR or 4DTDR intended for use in 4D dose calculation methods. The phantom allowed accurate quantification of a specific natural tissue hysteresis motion path using 4DCT and EMT-tracking. The overall average error of the evaluated 4DTDR_{hysteresis} to the measured data of the sinusoidal 4DCT was 0.9 mm and to the patient trace 4DCT within 1 mm. The 4DTDR_{hysteresis} traces matched 95% of the EMT points within 1 mm (sinusoidal) and within 4.5 mm (patient). The fit of an estimated motion trace to a real motion path as measured by 4DCT and EMT can be shown and validated. The average error presented applies to any point within the motion path.

^{a)} Author to whom correspondence should be addressed. Electronic mail: martin.szegedi@hci.utah.edu

¹J. Hinkle *et al.*, "4D MAP Image Reconstruction Incorporating Organ Motion," in *Information Processing in Medical Imaging - IPMI 2009*, Springer, p. 676–687.

²S. E. Geneser *et al.*, "Quantifying variability in radiation dose due to respiratory-induced tumor motion," *Med. Image Anal.* **15**(4), 640–649 (2011).

³G. G. Zhang *et al.*, "Dose mapping: Validation in 4D dosimetry with measurements and application in radiotherapy follow-up evaluation," *Comput. Methods Programs Biomed.* **90**(1), 25–37 (2008).

⁴V. Boldea *et al.*, "4D-CT lung motion estimation with deformable registration: Quantification of motion nonlinearity and hysteresis," *Med. Phys.* **35**, 1008–1018 (2008).

⁵Y. D. Mutaf, J. A. Antolak, and D. H. Brinkmann, "The impact of temporal inaccuracies on 4DCT image quality," *Med. Phys.* **34**, 1615–1622 (2007).

⁶K. K. Brock, "Results of a multi-institution deformable registration accuracy study (MIDRAS)," *Int. J. Radiat. Oncol., Biol., Phys.* **76**(2), 583–596 (2009).

⁷M. Szegedi *et al.*, "A proto-type design of a real tissue phantom for the validation of deformation algorithm and 4D dose calculations," *Phys. Med. Biol.* **55**(13), 3685–3699 (2010).

⁸S. S. Vedam *et al.*, "Quantifying the predictability of diaphragm motion during respiration with a noninvasive external marker," *Med. Phys.* **30**, 505–513 (2003).

⁹H. D. Kubo and B. C. Hill, "Respiration gated radiotherapy treatment: A technical study," *Phys. Med. Biol.* **41**, 83–92 (1996).

¹⁰H. D. Kubo *et al.*, "Breathing-synchronized radiotherapy program at the University of California Davis Cancer Center," *Med. Phys.* **27**, 346–353 (2000).

¹¹U. Langner and P. Keall, "Accuracy in the localization of thoracic and abdominal tumors using respiratory displacement, velocity, and phase," *Med. Phys.* **36**, 386–393 (2009).

¹²J. M. Balter *et al.*, "Accuracy of a wireless localization system for radiotherapy," *Int. J. Radiat. Oncol., Biol., Phys.* **61**(3), 933–937 (2005).

¹³S. Flampouri *et al.*, "Estimation of the delivered patient dose in lung IMRT treatment based on deformable registration of 4D-CT data and Monte Carlo simulations," *Phys. Med. Biol.* **51**(11), 2763–2779 (2006).

¹⁴E. Rietzel and G. T. Y. Chen, "Deformable registration of 4D computed tomography data," *Med. Phys.* **33**, 4423–4430 (2006).

¹⁵E. Heath *et al.*, "Quantification of accuracy of the automated nonlinear image matching and anatomical labeling (ANIMAL) nonlinear registration algorithm for 4D CT images of lung," *Med. Phys.* **34**, 4409–4421 (2007).

¹⁶A. Pevsner *et al.*, "Evaluation of an automated deformable image matching method for quantifying lung motion in respiration-correlated CT images," *Med. Phys.* **33**, 369–376 (2006).

¹⁷T. Rohlfing *et al.*, "Modeling liver motion and deformation during the respiratory cycle using intensity-based nonrigid registration of gated MR images," *Med. Phys.* **31**, 427 (2004).

¹⁸T. Rohlfing, C. M. WG O'Dell, Jr., and J. Zhong, "Modeling liver motion and deformation during the respiratory cycle using intensity-based free-form registration of gated MR images," *Medical Imaging: Visualization, Display, and Image-Guided Procedures, Proceedings of SPIE*, **4319**, 337–348 (2001).

¹⁹G. Remmert *et al.*, "Four-dimensional magnetic resonance imaging for the determination of tumour movement and its evaluation using a dynamic porcine lung phantom," *Phys. Med. Biol.* **52**(18), N401–N415 (2007).